Inorganic Chemistry

Article

pubs.acs.org/IC

Thermal and Light-Induced Spin Switching Dynamics in the 2D Coordination Network of $\{[Zn_{1-x}Fe_x(bbtr)_3](ClO_4)_2\}_\infty$: The Role of Cooperative Effects

Pradip Chakraborty,[†] Cristian Enachescu,[‡] Christophe Walder,[†] Robert Bronisz,[§] and Andreas Hauser*[,†]

[†]Département de Chimie Physique, Université de Genève, 30, quai Ernest-Ansermet, CH-1211 Genève, Switzerland

[‡]Faculty of Physics, Al. I. Cuza University, 700506 Iasi, Romania

[§]Faculty of Chemistry, University of Wroclaw, F. Joliot-Curie 14, 50-383 Wroclaw, Poland

ABSTRACT: The thermal spin transition, the photoexcitation, and the subsequent spin relaxation in the mixed crystal series of the covalently linked two-dimensional network $\{[Zn_{1-x}Fe_x(bbtr)_3](ClO_4)_2\}_\infty$ (x = 0.02−1, bbtr =1,4-di(1,2,3-triazol-1-yl)-butane) are discussed. In the neat compound, the thermal spin transition with a hysteresis of 13 K is accompanied by a crystallographic phase transition (Kusz, J.; Bronisz, R.; Zubko, M.; Bednarek, H. *Chem. Eur. J.* **2011**, *17*, 6807). In contrast, the diluted crystals with $x \leq 0.1$ stay essentially in the high-spin state down to low temperatures and show typical first order relaxation kinetics upon photoexcitation, and the structural phase transition is well separated from the spin transition. With increasing Fe(II) concentration, steeper thermal transitions and sigmoidal relaxation curves indicate increasingly important cooperative effects. Already at x = 0.38, the spin relaxation is governed by cooperative interactions between Fe(II) centers, and the crystallographic phase transition begins to influence the spin transition. The kinetic behavior of the thermal spin transition is reproduced within the framework of a dynamic mean-field model.

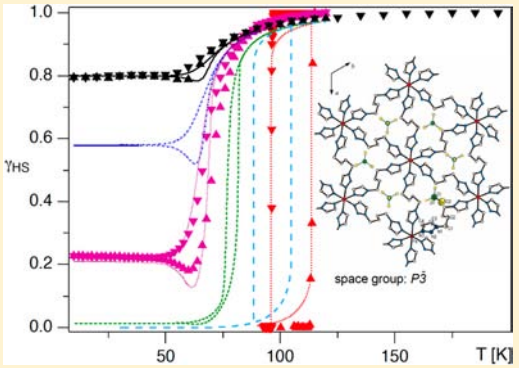

1. INTRODUCTION

Fe(II) spin-crossover complexes[1,2] are of current interest in chemistry and materials science, not only because of their intrinsic fundamental properties but also because of their potential applications as functional materials for the construction of sensors,[3−5] as well as memory[6] and display devices.[7,8] Spin-crossover phenomena imply labile electronic configurations between two spin manifolds of transition metal complexes having d^4−d^7 electronic configurations. In these complexes, the relative population of the two spin states is a function of various external perturbations such as temperature,[9] magnetic fields,[10,11] external pressure,[12,13] and light irradiation.[9,14]

For Fe(II), for which by far the largest number of spin-crossover complexes are known, the thermal spin transition takes place from the $^1A_1$ low-spin (LS) state as the quantum mechanical ground state populated at low temperature to the $^5T_2$ high-spin (HS) state at high temperature. The thermal transition, implying switching from the electronically non-degenerate LS state to the 15-fold quasidegenerate HS state, the latter having also a higher density of vibrational states, is therefore largely entropy driven, and the transition temperature is governed by the zero-point energy difference between those two spin manifolds.

Cooperative effects of elastic origin due to the large difference in metal−ligand bond length between the two states have been and continue to be of interest, as they constitute an essential ingredient for the macroscopic bistability[15−21] and memory effects needed for the potential application mentioned above.[3,6−8] Depending upon the nature of the ligand environment and interactions between the metal centers in the solid state, the thermal spin transition can thus be abrupt or gradual. If the interactions in the crystalline network are large enough, then the system is cooperative and the thermal transition can be accompanied by a hysteresis, very often involving a crystallographic phase transition.[22−25] The cooperative effects are influenced not only by the nature of intermolecular interactions, but also by the crystal structure,[26] and may lead to spontaneous symmetry breaking in double step transitions.[27,28]

Besides thermal control of the spin state, it is also possible to control the HS and LS populations with wavelength selective light irradiation. This phenomenon is commonly known as light induced excited spin state trapping (LIESST) for conversion from the LS to the HS state[14,29] or reverse-LIESST for HS to LS conversion.[30] Both phenomena have been extensively studied over two decades in Fe(II) based spin-crossover systems.[14,31,32] The relaxation from the light-induced metastable HS state back to the LS state is governed not only by

Received: May 15, 2012
Published: August 28, 2012

   dx.doi.org/10.1021/ic301006c | *Inorg. Chem.* 2012, 51, 9714−9722

external factors such as temperature or pressure, but also by some intrinsic factors as for instance the above-mentioned cooperative effects or the nature of the second coordination sphere.[33−36]

In the solid state, dilution with an inert ion forming mixed crystals with the spin-crossover ion has proved to be a powerful tool for the investigation of cooperative effects in spin-crossover compounds, in particular with Fe(II) as a central ion[16,37−40] but also in Prussian blue analogues.[41] Diluted spin-crossover systems may serve as reference systems in order to understand the thermal spin-crossover and relaxation behavior in the absence of long-range cooperative interactions as isolated molecular properties of a given complex. The influence of the inert metal ion is, however, not negligible. Previous experimental data show that larger dopants, such as Zn, stabilize the HS state by inducing so-called negative pressure, and consequently, the thermal transition is shifted toward lower temperatures as the dopant ratio increases.[16,37,42]

The simplest model for treating cooperative effects is the mean-field approach, successfully applied to a number of systems with moderate interaction parameters.[15,18,42−44] More complex approaches such as Ising-like models[45] or the recent mechano-elastic models[46,47] have also been considered in order to identify the effects of dilution on the LS⇔HS transition or to explain cooperative effects in spin-crossover compounds of other spin transition metal ions such as Mn(III).[48]

In previous work, we have shown that for the neat crystalline 2D polymer $\{[Fe(bbtr)_3](ClO_4)_2\}_\infty$ (bbtr = 1,4-di(1,2,3-triazol-1-yl)-butane) there is an abrupt LS⇔HS transition with a thermal hysteresis of 13 K and an accompanying crystallographic phase transition from $P\bar{3}$ to $P\bar{1}$,[25,49] while in the case of dilute $\{[Zn_{1-x}Fe_x(bbtr)_3](ClO_4)_2\}_\infty$ (x = 0.02), the Fe(II) centers stay essentially in the HS state down to 10 K[50] and the crystallographic phase transition is separated from the spin transition.[49] Kusz et al. conclude that the linear variations of the structural phase transition and the spin transition temperature as a function of iron concentration indicate that the structural phase transition does not directly trigger the spin transition but establishes a favorable environment for the spin transition to occur.[49] Moreover, in the diluted system, we have reported a variation of the intersystem-crossing rate constant for the LS→HS relaxation following the light-induced population of the LS state by 14 orders of magnitude between 40 and 220 K.[50] Herein, we present a detailed investigation of the thermal spin transition and subsequent LIESST, reverse-LIESST, and photoinduced spin relaxation behavior for the full series of mixed crystals of general composition $\{[Zn_{1-x}Fe_x(bbtr)_3](ClO_4)_2\}_\infty$, $0.02 \leq x \leq 1$.

2. EXPERIMENTAL SECTION

High quality mixed single crystals of $\{[Zn_{1-x}Fe_x(bbtr)_3](ClO_4)_2\}_\infty$ with x = 0.02, 0.1, 0.21, 0.38, 0.48, 0.68, 0.84, and 1 were synthesized and grown as previously described for the neat compound.[51] The effective concentrations in the mixed crystals were determined by ICP analysis.[49] In the compound $[Fe(bbtr)_3](ClO_4)_2$, the triazole based ligand acts as bridging ligand between two neighboring iron(II) centers, each of which is surrounded by six ligands. It forms a hexagonal 2D structure with the ClO_4^- anions between the layers. At room temperature the compound crystallizes in the space group $P\bar{3}$.[51] The Zn analogue as well as the mixed crystals crystallize in the same space group.[49]

The crystals are colorless in their HS state and reddish pink in the LS state. For optical and thermal investigations, crystals are mounted on copper plates with a hole of ~0.2 mm or less in diameter. For this, silver contact paste was placed around the hole, and then a small crystal (~0.3 × 0.3 × 0.1 mm^3) is placed over the hole carefully. This ensured good thermal contact of the crystal with the metal plate, which in turn was attached to the coldfinger of a closed cycle cryostat (Janis-Sumitomo SHI-4.5) operating between 4 and 400 K and equipped with a computer interfaced temperature controller (Lakeshore Model 331). For variable temperature absorption spectra in the UV−vis−NIR range, the cryostat was inserted into the sample compartment of a UV−vis−NIR spectrometer (Varian Cary 5000). For LIESST and reverse-LIESST experiments, a continuous diode pumped solid-state laser at 532 nm (ILEE VA−I-N-532) and a diode laser at 830 nm (ILEE Model Z40KV1) were used, respectively.

3. RESULTS AND DISCUSSION

3.1. Thermal Spin Transition, LIESST and Reverse-LIESST Behavior. Figures 1 and 2 show the single crystal

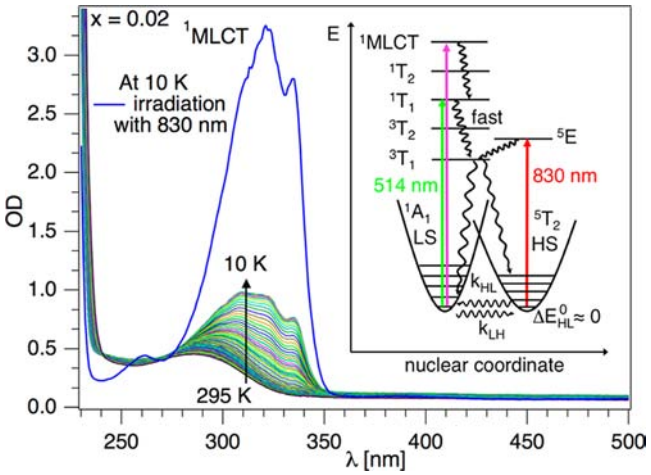

Figure 1. Single crystal absorption spectra as a function of temperature of $\{[Zn_{1-x}Fe_x(bbtr)_3](ClO_4)_2\}_\infty$, x = 0.02, with 0.1 K/min sweep rate on cooling from 295 to 10 K, and at 10 K after irradiation at 830 nm (blue solid line). Inset: Energy level scheme for LIESST and reverse-LIESST (adapted from ref 50).

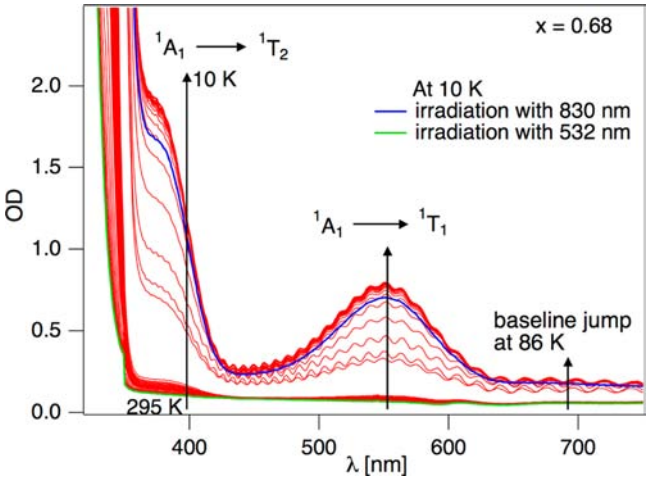

Figure 2. Single crystal absorption spectra as a function of temperature of $\{[Zn_{1-x}Fe_x(bbtr)_3](ClO_4)_2\}_\infty$, x = 0.68, with 0.1 K/min temperature sweep rate on cooling from 295 to 10 K, at 10 K after irradiation at 830 nm (blue solid line) and after irradiation at 532 nm (green solid line).

dx.doi.org/10.1021/ic301006c | Inorg. Chem. 2012, 51, 9714−9722

absorption spectra of $\{[Zn_{1-x}Fe_x(bbtr)_3](ClO_4)_2\}_\infty$ x = 0.02 and 0.68, respectively, as a function of temperature on cooling at a rate of 0.1 K/min. Depending upon the dilution, the evolution of either the ^{1}MLCT band centered at 320 nm (for x = 0.02) or the $^1A_1 \rightarrow {}^1T_1$ d−d band centered at 555 nm (for x = 0.68) may serve to monitor the spin state. In the absorption spectra of the very dilute system (Figure 1), the ^{1}MLCT band increases in intensity with decreasing temperature. In the absorption spectra of the more concentrated crystal (Figure 2), the same holds for the d−d band. In fact, at ∼86 K, the intensity of the d−d band appears in a discontinuous way and at the same time a baseline shift is observed similar to the observation previously reported for the neat compound at 100 K.[25] This baseline shift during the thermal spin transition on cooling from room temperature is attributed to increased diffuse scattering due to the formation of a domain structure of dimensions of the same order as the wavelength of the incoming light as a result of the crystallographic phase transition.[49] Furthermore, an interference pattern appears at the same temperature. This pattern is attributed to a cleaving of the crystal perpendicular to the c axis thus forming an air space operating as etalon for multiple reflections. This has also been observed for other higher Fe(II) concentrations.

Irradiation with light at 532 nm from a cw Nd:YAG laser at 10 K completely bleaches the characteristic LS absorption bands, that is, the ^{1}MLCT band for the dilute system and the $^1A_1 \rightarrow {}^1T_1$ band for the more concentrated systems, thus indicating a quantitative LS→HS transformation (LIESST). At 10 K the system is trapped in the metastable HS state for a very long time.[50] Subsequent prolonged irradiation with light at 830 nm from a diode laser, that is, into the near-infrared $^5T_2 \rightarrow {}^5E$ band of the HS species, reestablishes an LS steady state population of typically 85% for tetrazole and triazole based spin-crossover systems (reverse-LIESST).[14,30] From the corresponding spectra in Figures 1 and 2 it is thus obvious that upon cooling to 10 K at a temperature sweep rate of 0.1 K/min an LS fraction, γ_{LS}, of only 20% is obtained for x = 0.02, whereas in the more concentrated system the thermal transition is complete. Thus, for all concentrations the LS fraction at 10 K can be estimated with respect to the 85% LS population[14] after excitation at 830 nm, and the corresponding HS fraction as function of temperature, $\gamma_{HS}(T)$, can now be calculated according to

$$\gamma_{HS}(T) = \frac{OD_{LS}^{\lambda_{max}} - OD^{\lambda_{max}}(T)}{OD_{LS}^{\lambda_{max}} - OD_{HS}^{\lambda_{max}}} \quad (1)$$

where the optical densities are taken at the maximum of the ^{1}MLCT or d−d absorption bands of the LS species λ_{max}, and $OD_{LS}^{\lambda_{max}}$ and $OD_{HS}^{\lambda_{max}}$ are the optical densities at that wavelength for γ_{LS} = 1 and γ_{HS} = 1, respectively. $OD_{LS}^{\lambda_{max}}$ is taken either from the 10 K spectrum for the cases where the transition is complete or extrapolated from the reverse-LIESST spectrum for incomplete transitions. Accordingly, Figure 3 presents the thermal spin transition behavior of the mixed crystal series in both the cooling and the heating mode with a temperature sweep rate of 0.1 K/min. In more concentrated systems (x = 0.68, 0.84, and 1), the spin transition is complete and very abrupt and shows a discontinuity with a hysteresis. For x = 1 and 0.84, this discontinuity includes the complete spin transition; for x = 0.68 and 0.48, the discontinuity involves a partial crossover, followed by a more gradual transition at lower temperatures, with a residual HS fraction for x = 0.48 of ∼10%

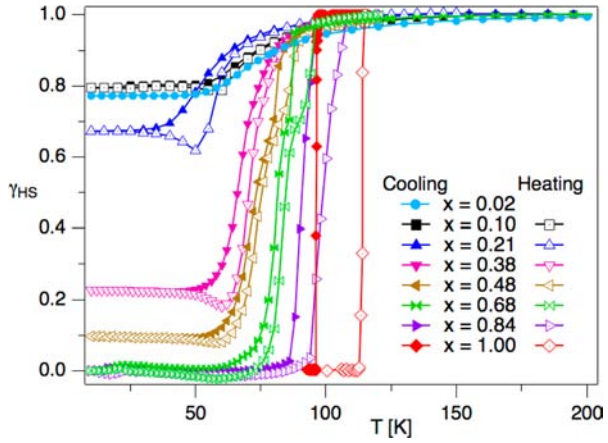

Figure 3. Thermal spin transition curves for the mixed crystal series $\{[Zn_{1-x}Fe_x(bbtr)_3](ClO_4)_2\}_\infty$, x = 0.02, 0.10, 0.21, 0.38, 0.48, 0.68, 0.84, and 1 obtained from optical absorption spectroscopy in cooling and heating mode (temperature sweep rate: 0.1 K/min).

at low temperatures. In accordance with the structural study of Kusz et al.,[49] the discontinuity with the hysteresis is attributed to the accompanying crystallographic phase transition. In dilute systems (x = 0.02, 0.10, 0.21, 0.38) the spin transition is gradual over the whole temperature range, and there is a residual HS fraction below 60 K. The fact that there is an apparent hysteresis with a decrease in the HS fraction on heating to below the initially reached value indicates that this is at least partially due to thermal quenching of the HS state. This low-temperature hysteresis is therefore a kinetic hysteresis with the system not in a thermodynamic equilibrium.

This is further borne out by the dependence on the temperature sweep rate. Figure 4 illustrates the effect of different temperature sweep rates on the spin transition behavior. For x = 0.1, the residual HS fraction of around 80% at low temperatures only depends very weakly on the temperature sweep rate, whereas for x = 0.21 it is 68% and 42% for scan rates of 0.1 and 0.02 K/min, respectively (Figure 4a). In addition, there is an apparent hysteresis in the transition curves with a further decrease of the HS fraction on heating in the range 40−60 K. This behavior is even more evident for x = 0.38 shown in Figure 4b. The inset of Figure 4b also shows the relaxation curves at a fixed temperature of 60 K observed upon fast cooling to this temperature and following irradiation at 532 nm. They both converge to the same HS fraction of 15%, which thus corresponds to the true value at thermodynamic equilibrium at this temperature and is just below the lowest value obtained on the heating branch for the slowest temperature sweep rate. This clearly identifies the kinetic origin of the apparent hysteresis observed in the thermal transition curves at comparatively low Fe(II) concentrations. Qualitatively this can be explained as follows: at around 60 K the HS→LS relaxation rate constant becomes so small that upon cooling a temperature sweep rate dependent HS fraction is frozen in below 60 K; that is, the smaller the sweep rate, the smaller the residual HS fraction. In the heating branch, the HS→LS relaxation then results in a further decrease of the HS fraction in the temperature range around 40−60 K, producing a shallow dip before increasing again. The dip is deeper and moves to higher temperatures for faster temperature sweep rates. Finally, for x = 0.48 (Figure 4c) the residual HS fraction is much smaller and again depends less on the temperature

dx.doi.org/10.1021/ic301006c | Inorg. Chem. 2012, 51, 9714−9722

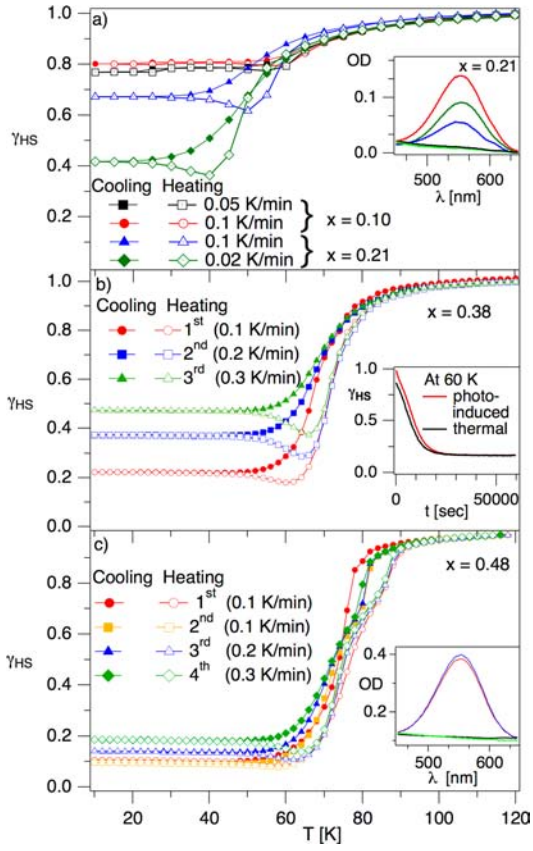

Figure 4. Effect of different temperature sweep rates on the thermal spin transition curves of (a) diluted systems $\{[Zn_{1-x}Fe_x(bbtr)_3](ClO_4)_2\}_\infty$, for $x = 0.10$ and $x = 0.21$. Inset: Absorption spectra for $x = 0.21$ at 10 K before irradiation 0.02 K/min (dark green solid line) and 0.1 K/min (blue solid line) and following irradiation at 532 nm (light green solid line) and 830 nm (red solid line) and at room temperature (black solid line). The latter spectra are used to calibrate the HS fraction. (b) For $x = 0.38$, for crystal Nr 1. Inset: $x = 0.38$ at 60 K, thermal (black solid line) relaxation after quenching from RT and photoinduced (red solid line) relaxation after quenching from RT followed by LIESST. (c) For $x = 0.48$. Inset: absorption spectra for $x = 0.48$ at 10 K before irradiation 0.1 K/min (blue solid line), and following irradiation at 532 nm (light green solid line) and 830 nm (red solid line) and at room temperature (black solid line) showing that the residual HS fraction on cooling at 0.1 K/min is around 10%.

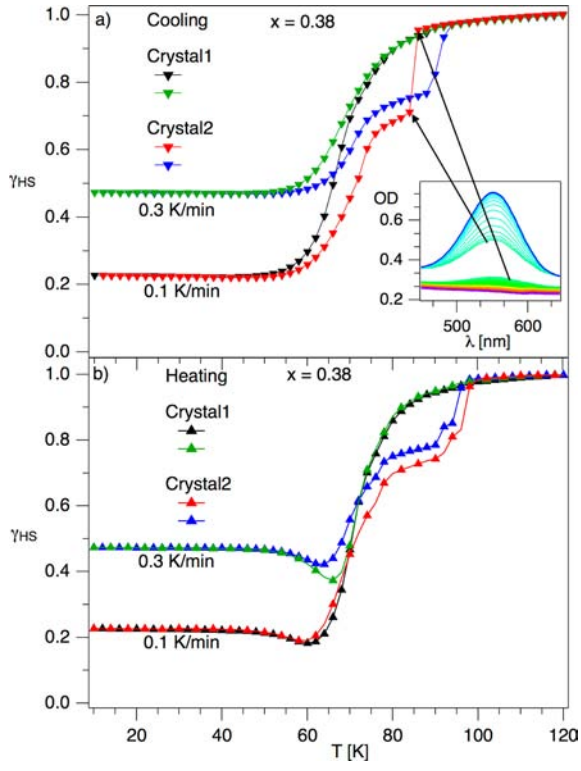

Figure 5. Comparison of the thermal spin transition curves for two crystals of $\{[Zn_{1-x}Fe_x(bbtr)_3](ClO_4)_2\}_\infty$, with $x = 0.38$, at different temperature sweep rates on (a) cooling and (b) heating (sequence: 1st cooling from RT and heating up to 120 at 0.1 K/min followed by 2nd cooling from 120 K and heating to 120 at 0.3 K/min). Inset a: single crystal absorption spectra for $\{[Zn_{1-x}Fe_x(bbtr)_3](ClO_4)_2\}_\infty$, with $x = 0.38$ for crystal Nr 2 on 1st cooling.

sweep rate. The small variation in the hysteresis at higher temperatures, involving a sudden jump in the HS fraction, does not so much depend on the temperature sweep rate but rather on the history of the sample. In section 3.2, the dependence of the thermal behavior on temperature sweep rate in a kinetic model will be analyzed quantitatively.

The insets of Figure 4a,c show the corresponding absorption spectra after different cooling cycles with different temperature sweep rates along with the photoinduced spectra at 10 K after irradiation with 532 nm (LIESST) and 830 nm (reverse-LIESST) that correspond to the reference spectra of 100% HS state and 85% steady-state LS fraction, respectively, used to normalize the transition curves as described above.

Figure 5a,b reproduces the thermal transition curves for temperature sweep rates of 0.1 and 0.3 K/min of crystal Nr 1 for $x = 0.38$ in cooling and sweeping modes, respectively. This figure also shows the transition curves under the same conditions for a second crystal, crystal Nr 2, from the same batch. The residual HS fractions of 22% and 46% for the two sweep rates are identical for the two crystals, and the shapes of the apparent hysteresis at low temperatures with the dips in the heating mode are very similar. However, for crystal Nr 2 there is jump in the baseline on the first cooling at ~85 K (inset of Figure 5a) with an accompanying jump in the HS fraction. On heating, the jump in the HS fraction occurs at 96 K. On further cycling the magnitude of the jump remains the same, but the hysteresis becomes progressively smaller. This behavior indicates that a small sample variability in the vicinity of $x = 0.38$ is sufficient to couple the crystallographic phase transition to the thermal spin transition. The baseline shift is thus again attributed to the abrupt increase of diffuse scattering induced by the symmetry breaking and random domain formation of the crystallographic phase transition.

3.2. Model. In order to simulate the thermal spin transition, a simple mean-field model was considered, which also takes into account the host lattice in the form of inert dopants. As the transition curves presented in the previous paragraph are strongly influenced by the temperature sweep rate, a dynamical treatment of the system is called for rather than simply determining the equilibrium populations as a function of temperature. This can be realized by using the classical master equation, including both HS→LS and LS→HS relaxation processes according to eq 2.

$$\frac{d\gamma_{HS}}{dT} = -k_{HL}(\gamma_{HS}, x, T)\gamma_{HS} + k_{LH}(\gamma_{HS}, x, T)(1 - \gamma_{HS}) \quad (2)$$

dx.doi.org/10.1021/ic301006c | Inorg. Chem. 2012, 51, 9714−9722

Here the LS→HS relaxation rate constant k_{LH} can be expressed as a function of the HS→LS relaxation rate constant k_{HL} and of the equilibrium constant K as $k_{LH} = k_{HL}K$ according to the principle of detailed balance.

For cooperative systems in the mean-field approximation and taking into account the concentration of the active Fe(II) complexes x, k_{HL} can be expressed with the autoaccelerating function according to eq 3.[52]

$$k_{HL}(\gamma_{HS}, x, T) = k^0_{HL}(x, T)\exp\left(\frac{\Gamma x(1-\gamma_{HS})}{k_B T}\right) \quad (3)$$

Here Γ is the interaction parameter and k^0_{HL} is the HS→LS relaxation rate constant at $\gamma_{HS} = 1$.

Simple thermodynamic considerations detailed elsewhere[16,37] on the basis of the classical model of Slichter and Drickamer[43] lead to the expression of eq 4 for the equilibrium constant of a mixed crystal series of a spin-crossover compound and an inert host lattice.

$$K = \frac{\gamma_{HS}}{1-\gamma_{HS}} = \exp\left(-\frac{\Delta H^0 - T\Delta S^0 - 2\Gamma x(\gamma_{HS} - \frac{1}{2}) - \Delta_M(1-x)}{k_B T}\right) \quad (4)$$

Here ΔH^0 and ΔS^0 are the standard enthalpy and entropy variations for the pure Fe(II) compound, and Δ_M introduces a correction to the enthalpy change for diluted systems. According to Spiering's lattice expansion model,[15,42] the so-called lattice shift, Δ_M, is proportional to the term $\Gamma(V_M - V_{LS})/(V_{HS} - V_{LS})$ where V_{HS}, V_{LS}, and V_M are the molecular volumes of the HS and the LS complexes and the inert host complex, respectively. With eqs 3 and 4, the macroscopic master eq 2 can be recast into eq 5.

$$\frac{d\gamma_{HS}}{dT} = -k^0_{HL}(x, T)\exp\left(\frac{\Gamma x(1-\gamma_{HS})}{k_B T}\right)\gamma_{HS} + k^0_{HL}(x, T) \exp\left(\frac{\Gamma x(1-\gamma_{HS})}{k_B T}\right) \exp\left(-\frac{\Delta H^0 - T\Delta S^0 - 2\Gamma x(\gamma_{HS} - \frac{1}{2}) - \Delta_M(1-x)}{k_B T}\right)(1-\gamma_{HS}) \quad (5)$$

As bigger dopants stabilize the HS state, while smaller dopants stabilize the LS state and therefore increase the initial HS→LS relaxation rate for diluted compounds, the relaxation rate constant at $\gamma_{HS} = 1$, k^0_{HL}, can be further expressed as a function of the dilution.

$$k^0_{HL}(x, T) = k^0_{HL}(x \to 0, T)\exp\left(\frac{(\Gamma - \Delta_M)x}{k_B T}\right) \quad (6)$$

In the particular case of dilution in the Zn(II) host, Zn(II) having an ionic radius which is approximately the same as the Fe(II) radius in the HS state, Γ will equal the dopant interaction parameter Δ_M,[15] and therefore $k^0_{HL}(x,T) \approx k^0_{HL}(x \to 0,T)$. In theory also the acceleration factor would have to be considered differently in the tunneling and in the activated region. However, eq 3 is a very good approximation down to 40 K for systems with a small zero-point energy difference.[14]

In the simulations presented below, the values for $k^0_{HL}(x \to 0,T)$ have been taken from the experimental data obtained for the diluted (x = 0.02) complex.[50] This ensures a correct description of the rate constant in the region between low-temperature tunneling and thermal activation, where Arrhenius behavior is not justified. Figure 6a presents experimental and simulated thermal transition curves for different values of x.

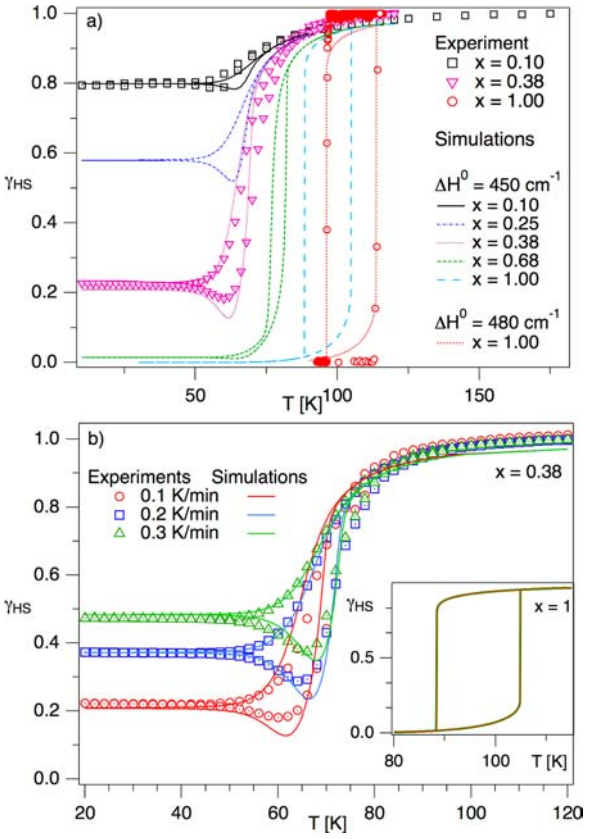

Figure 6. (a) Dependence of the dynamic thermal transition curves in mixed crystal systems for different values of x. The parameters used in the simulations are ΔH^0 = 450 cm^{-1}, ΔS^0 = 4.6 cm^{-1}/K, and $\Gamma = \Delta_M$ = 220 cm^{-1}. For the pure Fe(II) compound the value of ΔH^0 = 480 cm^{-1}. (b) Dependence of the dynamic thermal transition curves in the diluted system with x = 0.38 on the temperature sweep rate: experimental data (open symbols) and simulations (full curves). Inset: simulated thermal hysteresis for the pure Fe(II) compound at two temperature sweep rates.

The latter have been computed at the experimental temperature sweep rate dT/dt = 0.1 K/min. Only the experimental data, except for x = 1, not evidently affected by the crystallographic phase transformation are plotted in Figure 6a. The same values for the physical parameters ΔH^0 = 450 cm^{-1}, ΔS^0 = 4.6 cm^{-1}/K, and $\Gamma = \Delta_M$ = 220 cm^{-1} have been used in the simulations for all curves, except for the pure Fe(II) compound where the enthalpy difference had to be increased to ΔH^0 = 480 cm^{-1} in order to obtain a good fit to the experimental data. This enthalpy variation is attributed to a contribution from the crystallographic phase transition just around the thermal spin transition, which can modify the physical parameters of the system. The value of 220 cm^{-1} for Γ in the pure Fe(II) system is larger than the critical value $\Gamma_c = 2k_B T_{1/2} \approx$ 140 cm^{-1}, or putting it the other way round, in the mixed system, a thermodynamically controlled hysteresis is expected for x > ~0.6 even in the absence of any crystallographic phase transition. Thus, the hysteresis of around 3 K in the thermal transition curve below the jump due to the crystallographic phase transition of the x = 0.68 sample can also be attributed to a thermodynamic hysteresis (see Figure 3).

dx.doi.org/10.1021/ic301006c | Inorg. Chem. 2012, 51, 9714−9722

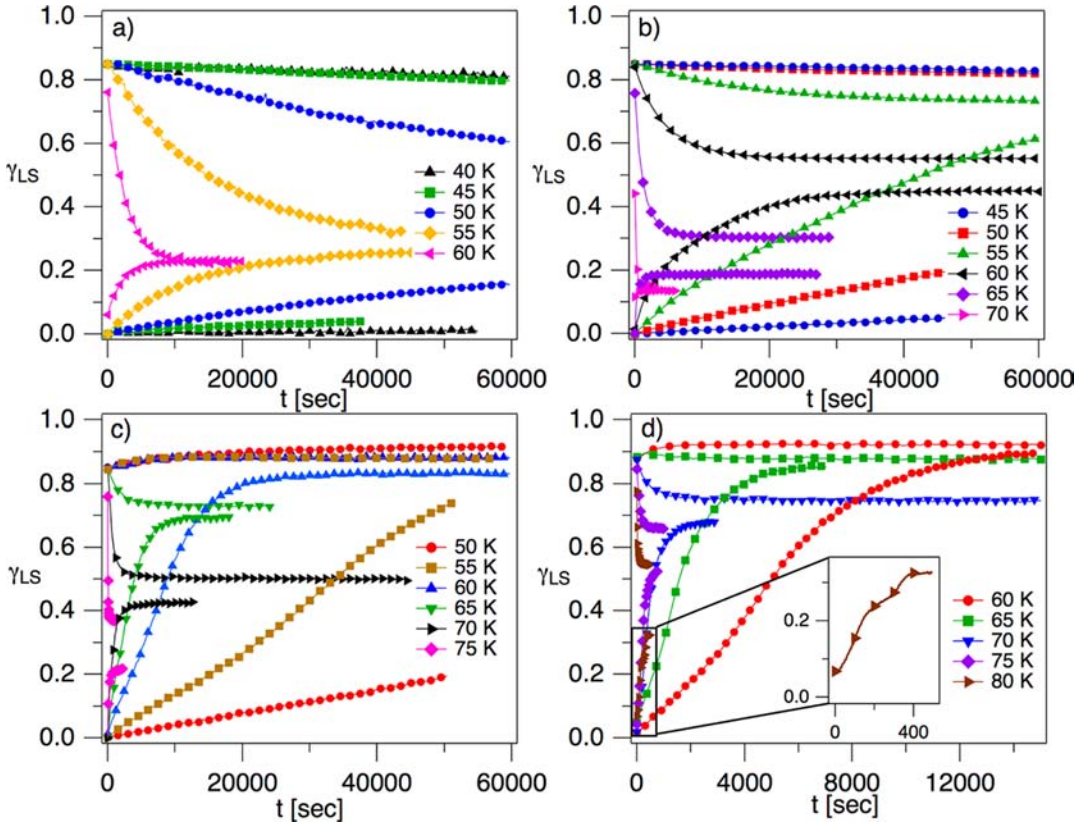

Figure 7. HS→LS and LS→HS relaxation curves as a function of temperature determined from full absorption spectra after irradiation at 532 and 830 nm, respectively: (a) x = 0.1, (b) x = 0.21, (c) x = 0.38 (crystal Nr 1), and (d) x = 0.48.

Figure 6b describes the experimental and simulated thermal transition curves for x = 0.38 at several temperature sweep rates. As in the experimental data, in the simulations the HS state population trapped during cooling increases with the temperature sweep rate. Both in the experimental and simulation situations, the dips on the heating branch move toward higher temperatures with the increasing sweep rate and their depths are enhanced. For a quick comparison, we present in the inset of Figure 6b the kinetic hysteresis loops calculated for the pure Fe(II) compound at the extreme temperature sweeping rates in the main figure. In this case, as the relaxation rates are much higher (around 10^3 at 100 K[50]) the hysteresis loops no longer depend on the temperature sweep rate.

3.3. HS→LS and LS→HS Relaxation Behavior. As specified in the Introduction, the shape of the relaxation curves, either following irradiation or thermal quenching, is particularly important in order to understand the nature of the relaxation mechanism. For diluted systems the relaxation is expected to be single exponential, whereas with increasing Fe(II) concentration it often becomes sigmoidal corresponding to the fact that initial slow nucleation is followed by the fast self-accelerating components. Relaxation curves thus directly reflect the degree of cooperativity.

Figure 7a–d illustrate the photoinduced HS→LS and LS→HS relaxation behavior as a function of temperature below and in the vicinity of the thermal spin transition for the mixed crystals with x = 0.1, 0.21, 0.38 (crystal Nr 1) and 0.48 of the title complex. The former all begin from full conversion to the HS state by irradiation at 532 nm, and the latter from the 85% steady state LS fraction obtained by irradiation at 830 nm.

In previous work, we have shown that for the very dilute system (x = 0.02) the spin relaxation to the global thermodynamic equilibrium state is indeed single exponential and becomes very slow below 70 K, and the thermodynamic equilibrium can be approached from either side.[50] For the diluted but slightly more concentrated system (x = 0.1, Figure 7a), the relaxation is still close to single exponential and thus dominated by a stochastic evolution of the HS fraction. In addition, the system relaxes to the thermodynamic equilibrium with the same rate constant irrespective of the starting conditions. With increasing Fe(II) concentration (x = 0.21, 0.38, and 0.48, Figure 7b–d, respectively), the relaxation curves change in shape, first deviating from single exponential and then becoming more and more sigmoidal. Additionally, HS→LS and LS→HS relaxation curves at a given temperature within the range of the thermal transition end up at different HS fractions depending upon the initial state. Whereas the former is expected on the basis of the increase of the effective interaction constant with Fe(II) concentration, the latter is difficult to explain in the mean-field picture as it implies hysteresis behavior even for diluted systems for which the effective interaction constant is below the critical mean-field value. This could be tentatively assigned to nonrandom distributions, concentration gradients, and clustering of the Fe(II) centers during crystal growth.

Moreover, for higher Fe(II) concentrations, the crystallographic phase transition also plays an important role during photoinduced spin relaxation in the corresponding temperature interval. The inset of Figure 7d shows a stepped and sigmoidal relaxation recorded for x = 0.48 in the vicinity of the crystallographic phase transition temperature, which is proof

dx.doi.org/10.1021/ic301006c | Inorg. Chem. 2012, 51, 9714–9722

that in this region the kinetics of spin transition is influenced by the reorganization of the respective HS and LS lattices.

Figure 8 shows the photoinduced HS→LS relaxation curves of the mixed crystal system with x = 0.68 at different

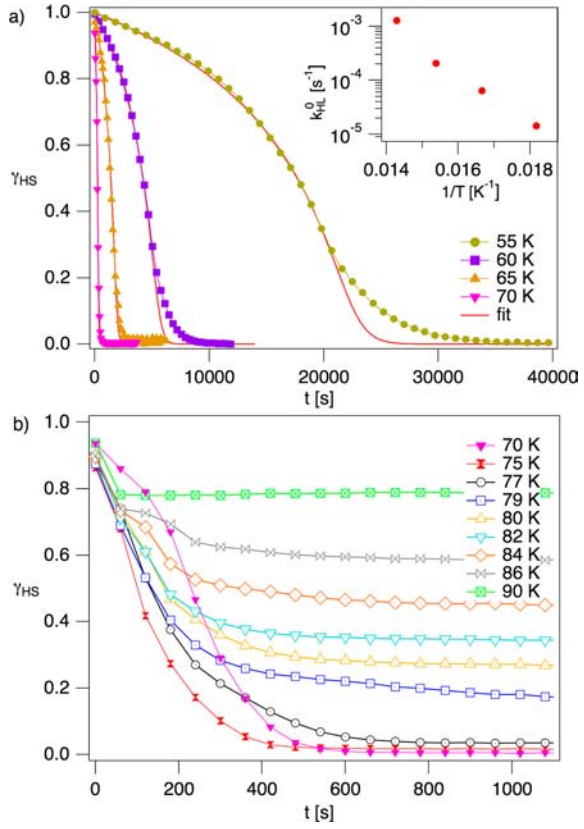

Figure 8. HS→LS relaxation behavior of $\{[Zn_{1-x}Fe_x(bbtr)_3](ClO_4)_2\}_\infty$, x = 0.68, following LIESST at various temperatures determined from full absorption spectra: (a) below the thermal transition temperature, red lines show best fit with Γ = 220 cm^{-1} taken from section 3.2 and $k^0_{HL}(T)$ as free parameter (inset: $k^0_{HL}(T)$ versus 1/T) (b) in the temperature interval of the thermal transition.

temperatures from 55 K up to the transition temperature. For this value of x, only HS→LS relaxation curves via LIESST can be recorded below 75 K. The sigmoidal shape of the corresponding curves clearly demonstrates the importance of cooperative effects for the photoinduced spin relaxation. These curves are very well described by the self-accelerating rate constant of eq 3 as demonstrated by the calculated curves included in Figure 8a using the value of Γ = 220 cm^{-1} as derived in section 3.2 and $k^0_{HL}(T)$ as the only adjustable parameter. The deviation from the mean-field behavior with a slower tail toward the end of the relaxation curves can be attributed to a comparatively small inhomogeneous distribution of zero-point energies in the mixed crystals.[18,53] The inset of Figure 8a shows $k^0_{HL}(T)$ versus 1/T. The values are in line with the assumption that for Zn dilution $k^0_{HL}(T)$ does not depend on x insofar as they are very close to the ones determined for the very dilute system with x = 0.02.[50] Comparison with the HS→LS relaxation curves for x = 1 shows that this is also the case for $k^0_{HL}(T)$ of the neat compound.[25] However, with respect to the shape of the relaxation curves, although those for the neat compound start off according to the mean-field model, they accelerate much faster than predicted.[50] This has been attributed to a nucleation and growth mechanism, which here is inhibited by the presence of the inert Zn dopants in the mixed crystals even at moderate dopant concentrations.

With increasing temperature, the relaxation for x = 0.68 initially becomes faster and is dominated by the sigmoidal behavior up to 75 K. As illustrated in Figure 8b, it becomes slower again as the temperature approaches the temperature of the jump in the thermal spin transition. This may be attributed to the presence of non-negligible short-range interactions leading to the formation of a domain structure as previously observed in neat crystals.[25]

Finally, Figure 9 shows the HS→LS relaxation behavior after thermal quenching from RT to the various experimental

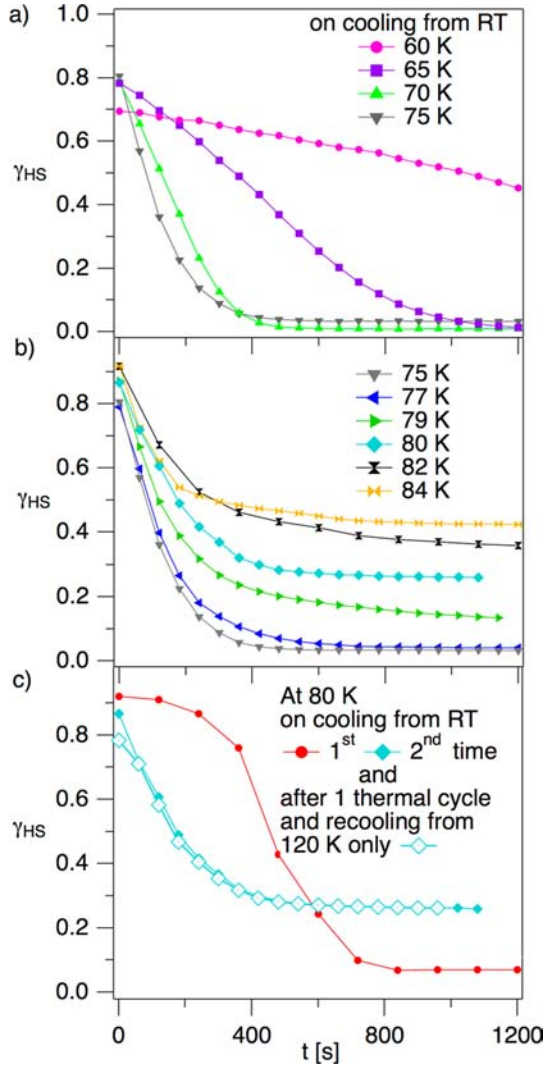

Figure 9. HS→LS relaxation behavior of $\{[Zn_{1-x}Fe_x(bbtr)_3](ClO_4)_2\}_\infty$, x = 0.68, following rapid thermal quenching from RT to various experimental temperatures determined from full absorption spectra.

temperatures in the vicinity of the thermal spin transition temperature for x = 0.68. Before each thermal relaxation measurement, the crystal was taken back to RT in order to anneal it to its initial phase. The initial HS fraction is somewhat less than unity, as despite the rapid cooling some complexes find time to relax to the LS state. In the temperature range 60–75 K (Figure 9a) the curves show the same sigmoidal shape as for the relaxation of the light-induced HS state. In particular the

dx.doi.org/10.1021/ic301006c | Inorg. Chem. 2012, 51, 9714–9722

curves at 65 K are almost superimposable when the one of the thermal quenching is displaced on the time axis such that its initial value of the HS fraction of 80% lies on the curve after irradiation. This indicates that below the thermal transition temperature and at early times the thermal relaxation occurs as a random process in accordance with the mean-field description. As for the relaxation of the light-induced HS state, with increasing temperature (Figure 9b), relaxation curves become less sigmoidal and the HS population finally evolves toward the thermal equilibrium in an almost single exponential way close to the temperature of 85 K where the jump in the thermal transition curve is observed. Despite this there is evidence of the influence of the crystallographic phase transition and the resulting deterioration in crystal quality on the thermal relaxation (Figure 9c). When a fresh crystal is rapidly cooled to 80 K for the first time, the thermal relaxation has the characteristics of a nucleation and growth process. At the same time there is an increase in diffuse scattering and the crystal develops microscopic cracks. On subsequent cooling to 80 K either after heating back up to RT or only to 120 K, the relaxation curves are closer to exponential and the final HS fraction at that temperature is somewhat higher. This indicates that on the first cooling the relaxation is governed by the kinetics of the crystallographic phase transition, which induces the microscopic cracks and therefore a domain structure. On subsequent cooling, the relaxation is governed by the HS→LS relaxation, which occurs independently in each domain.

4. CONCLUSIONS

In the concentrated systems, cooperative effects are very strong and are strongly influenced by a crystallographic phase transition. In the dilute systems they are weak and the spin transition is shifted to lower temperatures such that it becomes incomplete. In addition to a partial thermal quenching, the residual HS fraction could also be due to the vibronic structure of the HS spin state resulting from splittings due to the trigonal ligand field and spin−orbit coupling, and possibly to an inhomogeneous distribution of the zero-point energy difference between the two spin states. Kinetic trapping and memory effects were also observed in the intermediate mixed crystals. These are associated with crystallographic phase transitions and the kinetics competing with comparatively slow kinetics of the intersystem crossing process at the molecular level and the macroscopic crystallographic phase transition. The latter depends upon sample history and crystal quality. Thus, processes governed by it show a non-negligible variability and do not conform to mean-field behavior. On the other hand, for relaxation processes governed solely by the intersystem crossing process, cooperative effects can be satisfactorily modeled within the mean-field approximation. The detailed investigation of LIESST, reverse-LIESST, and the HS⇔LS relaxation dynamics in the $\{[Zn_{1-x}Fe_x(bbtr)_3](ClO_4)_2\}_\infty$ mixed crystal series presented here can thus help us to understand the interplay between the spin transition and crystallographic phase transitions and be instrumental for the design of highly cooperative systems.

AUTHOR INFORMATION

Corresponding Author

*E-mail: andreas.hauser@unige.ch.

Notes

The authors declare no competing financial interest.

ACKNOWLEDGMENTS

This work was supported by the Swiss National Science Foundation (Grant 200020-137567), the Romanian National Research Council (Grants PCCE 9/2010 and TE 185/2010), and the Ministry of Science and Higher Education of Poland (Grant 2493/B/H03/2008/34).

REFERENCES

(1) Spin Crossover in Transition Metal Compounds I−III. In *Topics in Current Chemistry*; Gütlich, P., Goodwin, H. A., Eds.; Springer-Verlag: Berlin, Germany, 2004; Vols. *233*−*235*.
(2) Bousseksou, A.; Molnar, G.; Salmon, L.; Nicolazzi, W. *Chem. Soc. Rev.* **2011**, *40*, 3313.
(3) Ohba, M.; Yoneda, K.; Agusti, G.; Muñoz, M. C.; Gaspar, A. B.; Real, J. A.; Yamasaki, M.; Ando, H.; Nakao, Y.; Sakaki, S.; Kitagawa, S. *Angew. Chem., Int. Ed.* **2009**, *48*, 4767.
(4) Renz, F.; de Souza, P. A.; Klingelhöfer, G.; Goodwin, H. A. *Hyperfine Interact.* **2002**, *139* − *140*, 699.
(5) Linares, J.; Codjovi, E.; Garcia, Y. *Sensors* **2012**, *12*, 4479.
(6) Létard, J. F.; Guionneau, P.; Goux-Capes, L. *Top. Curr. Chem.* **2004**, *235*, 221.
(7) Matsuda, M.; Isozaki, H.; Tajima, H. *Thin Solid Films* **2008**, *517*, 1465.
(8) Matsuda, M.; Tajima, H. Patent JP2009212164-A, 2009.
(9) Gütlich, P.; Hauser, A.; Spiering, H. *Angew. Chem.* **1994**, *106*, 2971. Gütlich, P.; Hauser, A.; Spiering, H. *Angew. Chem., Int. Ed.* **1994**, *33*, 2024.
(10) Bousseksou, A.; Negre, N.; Goiran, M.; Salmon, L.; Tuchagues, J.-P.; Boillot, M.-L.; Boukheddaden, K.; Varret, F. *Eur. Phys. J. B* **2000**, *13*, 451.
(11) Bonhommeau, S.; Molnar, G.; Goiran, M.; Boukheddaden, K.; Bousseksou, A. *Phys. Rev. B* **2006**, *74*, 064424.
(12) Jeftic, J.; Hauser, A. *J. Phys. Chem. B* **1997**, *101*, 10262.
(13) Gütlich, P.; Ksenofontov, V.; Gaspar, A. B. *Coord. Chem. Rev.* **2005**, *249*, 1811.
(14) Hauser, A. *Top. Curr. Chem.* **2004**, *234*, 155.
(15) Spiering, H.; Meissner, E.; Köppen, H.; Müller, E. W.; Gütlich, P. *Chem. Phys.* **1982**, *68*, 65.
(16) (a) Martin, J. P.; Zarembowitch, J.; Dworkin, A.; Haasnoot, J. G.; Codjovi, E. *Inorg. Chem.* **1994**, *33*, 2617. (b) Martin, J. P.; Zarembowitch, J.; Bousseksou, A.; Dworkin, A.; Haasnoot, J. G.; Varret, F. *Inorg. Chem.* **1994**, *33*, 6325.
(17) (a) Hinek, R.; Spiering, H.; Gütlich, P.; Hauser, A. *Chem.—Eur. J.* **1996**, *2*, 1435. (b) Hinek, R.; Spiering, H.; Gütlich, P.; Hauser, A. *Chem.—Eur. J.* **1996**, *2*, 1427.
(18) Hauser, A.; Jeftic, J.; Romstedt, H.; Hinek, R.; Spiering, H. *Coord. Chem. Rev.* **1999**, *190*−*192*, 471.
(19) Köhler, C. P.; Jakobi, R.; Meissner, E.; Wiehl, L.; Spiering, H.; Gütlich, P. *J. Phys. Chem. Solids* **1990**, *51*, 239.
(20) Cobo, S.; Ostrovskii, D.; Bonhommeau, S.; Vendier, L.; Molnar, G.; Salmon, L.; Tanaka, K.; Bousseksou, A. *J. Am. Chem. Soc.* **2008**, *130*, 9019.
(21) Chakraborty, P.; Bronisz, R.; Besnard, C.; Guénée, L.; Pattison, P.; Hauser, A. *J. Am. Chem. Soc.* **2012**, *134*, 4049.
(22) Kusz, J.; Zubko, M.; Neder, R. B.; Gütlich, P. *Acta Crystallogr., Sect. B* **2012**, *68*, 40.
(23) Lakhloufi, S.; Guionneau, P.; Lemee-Cailleau, M. H.; Rosa, P.; Létard, J. -F. *Phys. Rev. B* **2010**, *82*, 132104.
(24) Franke, P. L.; Haasnoot, J. G.; Zuur, A. P. *Inorg. Chim. Acta* **1982**, *59*, 5.
(25) (a) Krivokapic, I.; Enachescu, C.; Bronisz, R.; Hauser, A. *Chem. Phys. Lett.* **2008**, *455*, 192. (b) Krivokapic, I.; Enachescu, C.; Bronisz, R.; Hauser, A. *Inorg. Chim. Acta* **2008**, *361*, 3616.
(26) Halcrow, M. A. *Chem. Soc. Rev.* **2011**, *40*, 4119.
(27) Chernyshov, D.; Hostettler, M.; Törnroos, K. W.; Bürgi, H.-B. *Angew. Chem.* **2003**, *115*, 3955; *Angew. Chem., Int. Ed.* **2003**, *42*, 3825.
(28) Adams, C. J.; Muñoz, M. C.; Waddington, R. E.; Real, J. A. *Inorg. Chem.* **2011**, *50*, 10633.

(29) Decurtins, S.; Gütlich, P.; Köhler, C. P.; Spiering, H.; Hauser, A. *Chem. Phys. Lett.* **1984**, *105*, 1.
(30) (a) Hauser, A. *Chem. Phys. Lett.* **1986**, *124*, 543. (b) Hauser, A. *J. Chem. Phys.* **1991**, *94*, 2741.
(31) (a) Decurtins, S.; Gütlich, P.; Hasselbach, K. M.; Hauser, A.; Spiering, H. *Inorg. Chem.* **1985**, *24*, 2174. (b) Decurtins, S.; Gütlich, P.; Köhler, C. P.; Spiering, H. *J. Chem. Soc., Chem. Commun.* **1985**, 430.
(32) (a) Létard, J. F. *J. Mater. Chem.* **2006**, *16*, 2550. (b) Létard, J. F.; Chastanet, G.; Nguyen, O.; Marcen, S.; Marchievie, M.; Guionneau, P.; Chasseau, P. *Monatsh. Chem.* **2003**, *134*, 165.
(33) Boillot, M.-L.; Zarembowitch, J.; Sour, A. *Top. Curr. Chem.* **2004**, *234*, 261−276.
(34) (a) Boillot, M.-L.; Pillet, S.; Tissot, A.; Rivière, E.; Claiser, N.; Lecomte, C. *Inorg. Chem.* **2009**, *48*, 4729. (b) Tissot, A.; Boillot, M.-L.; Pillet, S.; Codjovi, E.; Boukheddaden, K.; Lawson Daku, L. M. *J. Phys. Chem. C* **2010**, *114*, 21715.
(35) Hasegawa, Y.; Takahashi, K.; Kume, S.; Nishihara, H. *Chem. Commun.* **2011**, *47*, 6846.
(36) Takahashi, K.; Hasegawa, Y.; Sakamoto, R.; Nishikawa, M.; Kume, S.; Nishibori, E.; Nishihara, H. *Inorg. Chem.* **2012**, *51*, 5188.
(37) Jakobi, R.; Spiering, H.; Wiehl, L.; Gmelin, E.; Gütlich, P. *Inorg. Chem.* **1988**, *27*, 1823.
(38) Enachescu, C.; Linares, J.; Varret, F. *J. Phys.: Condens. Matter* **2001**, *13*, 2481.
(39) Baldé, C.; Desplanches, C.; Grunert, M.; Wei, Y.; Gütlich, P.; Létard, J.-F. *Eur. J. Inorg. Chem.* **2008**, 5382.
(40) Yu, Z.; Kuroda-Sowa, T.; Kume, H.; Okubo, T.; Maekawa, M.; Munakata, M. *Bull. Chem. Soc. Jpn.* **2009**, *82*, 333.
(41) Cafun, J. D.; Londinière, L.; Rivière, E.; Bleuzen, A. *Inorg. Chim. Acta* **2008**, *361*, 3555.
(42) Spiering, H. *Top. Curr. Chem.* **2004**, *235*, 171.
(43) Slichter, C. P.; Drickamer, H. G. *J. Chem. Phys.* **1972**, *56*, 2142.
(44) Varret, F.; Boukheddaden, K.; Codjovi, E.; Enachescu, C.; Linares, J. *Top. Curr. Chem.* **2004**, *234*, 199.
(45) Hôo, B.; Boukheddaden, K.; Varret, F. *Eur. Phys. J. B* **2000**, *17*, 449.
(46) (a) Enachescu, C.; Stoleriu, L.; Stancu, A.; Hauser, A. *Phys. Rev. Lett.* **2009**, *102*, 257204. (b) Enachescu, C.; Stoleriu, L.; Stancu, A.; Hauser, A. *J. Appl. Phys.* **2011**, *109*, 07B111.
(47) Nishino, M.; Enachescu, C.; Miyashita, S.; Boukheddaden, K.; Varret, F. *Phys. Rev. B* **2010**, *82*, 020409.
(48) Klokishner, S. I.; Roman, M. A.; Reu, O. S. *Inorg. Chem.* **2011**, *50*, 11394.
(49) Kusz, J.; Bronisz, R.; Zubko, M.; Bednarek, H. *Chem.—Eur. J.* **2011**, *17*, 6807.
(50) (a) Krivokapic, I.; Chakraborty, P.; Enachescu, C.; Bronisz, R.; Hauser, A. *Angew. Chem., Int. Ed.* **2010**, *49*, 8509. (b) Krivokapic, I.; Chakraborty, P.; Enachescu, C.; Bronisz, R.; Hauser, A. *Inorg. Chem.* **2011**, *50*, 1856.
(51) Bronisz, R. *Inorg. Chem.* **2005**, *44*, 4463.
(52) (a) Hauser, A.; Gütlich, P.; Spiering, H. *Inorg. Chem.* **1986**, *25*, 4245. (b) Hauser, A *Chem. Phys. Lett.* **1992**, *192*, 65.
(53) Desaix, A.; Roubeau, O.; Jeftic, J.; Haasnoot, J. G.; Boukheddaden, K.; Codjovi, E.; Linares, J.; Nogues, M.; Varret, F. *Eur. Phys. J. B* **1998**, *6*, 183.